Three, four and five interacting electrons in a spherical box: an exact diagonalization study extended

2004 J. Phys.: Condens. Matter 16 7979

(http://iopscience.iop.org/0953-8984/16/45/020)

INSTITUTE OF PHYSICS PUBLISHING JOURNAL OF PHYSICS: CONDENSED MATTER

J. Phys.: Condens. Matter **16** (2004) 7979–7994 PII: S0953-8984(04)82913-8

Three, four and five interacting electrons in a spherical box: an exact diagonalization study extended

D C Thompson[1] **and A Alavi**

Cambridge University Centre for Computational Chemistry, Lensfield Road, Cambridge CB2 1EW, UK

E-mail: asa10@cam.ac.uk

Received 2 July 2004, in final form 2 September 2004
Published 29 October 2004
Online at stacks.iop.org/JPhysCM/16/7979
doi:10.1088/0953-8984/16/45/020

Abstract

We study the problem of N electrons confined to a hard three-dimensional spherical box, for $N = 3, 4$ and 5. Full-configuration interaction and Hartree–Fock calculations have been performed. We report energies, densities, second-order density matrices and exchange–correlation holes. In the $N = 4$ system, we observe a spin transition as the radius R of the sphere is increased, changing the ground state from ^{3}P to ^{5}S. The $N = 3$ and 5 systems remain ^{2}P and ^{4}S, respectively, for all R investigated. Pair-correlation functions and physical exchange–correlation holes have been computed over a regime in which the systems transform from liquid droplets to Wigner molecules. These functions show marked, yet characteristic, changes in this regime. By computing $|E_c/E|$, where E_c is the correlation energy defined with respect to the unrestricted Hartree–Fock solution, we show that the maximum relative error in the UHF energies occurs in this crossover regime. These systems provide challenging benchmarks for post-Hartree–Fock and density functional theory methods.

(Some figures in this article are in colour only in the electronic version)

1. Introduction

Interacting electron systems which are amenable to exact solution provide an interesting and uniquely detailed picture regarding electron correlation, as well as stringent quantitative tests of approximations, e.g. Hartree–Fock (HF) theory [1, 2] or density functional theory (DFT) [3, 4], to which one usually resorts in order to tackle realistic systems. In particular the full-configuration interaction method (FCI), if carried out to convergence, provides unbiased correlated wavefunctions which can be analysed in terms of pair-correlation functions, the associated exchange–correlation holes and natural orbitals. Whilst the wavefunction itself is a

[1] Present address: Department of Chemistry, McMaster University, 1280 Main Street West, Hamilton, ON, Canada.

cumbersome entity to deal with, these reduced quantities essentially completely characterize the correlation in the system. They are, however, far from simple. Being able to 'look' at these functions, and analyse them, is an exciting prospect. It is not even necessary to restrict to ground states: a powerful feature of the FCI method is that, with essentially no additional computational effort, one can obtain low lying excited states as well. Understanding the behaviour of the exact solutions is an important step towards modelling the correlation functions quantitatively. Since any approximate functional has an underlying (and usually unknown) pair-correlation function, an improved understanding may well help with the ultimate goal of designing more accurate functionals.

Of the various model electron systems, perhaps the best studied of all is the uniform electron gas (UEG), which is characterized by the single parameter r_s. The local density approximation is rooted in this system which, for metallic systems in particular, has been singularly successful. Yet, it is a curious system: the interacting ground state density is the same as the non-interacting density at all r_s! In fact, it has excited states which are uniform as well. Moving towards an *inhomogeneous* system still characterized by a single parameter is clearly desirable. Consider, for example, the Hooke's law atom, or Harmonium, system of electrons confined by a parabolic potential of given strength. This analytically solvable model [5, 6] has been used to great effect to assess DFT and HF theories alike [5, 7, 8] and admits testing in both the weakly and strongly correlated regimes. In a recent paper Taut *et al* extended the two-electron Harmonium to a three-electron system, using perturbation techniques—it is remarked that the method employed is generalizable to an arbitrary number of electrons [9]. It is with a somewhat similar motivation that we present this work.

Recent work by the present authors and, concurrently, Jung and Alvarellos has looked at a two-electron system confined by an infinite hard walled box of either cuboidal [10] or spherical [11, 12] shape. We have also reported in a letter an extension of the spherical box up to five electrons [13]. Here we give a more complete account of this work, concentrating mainly on full-configuration interaction calculations. In this model, the strength of the correlation between the particles is mediated through the radius R of the confining sphere. The accurate solutions to the two-electron spherical problem have been compared to both HF [14] and commonly used density functional solutions [15] where it is observed that the local density, generalized gradient and meta-generalized gradient approaches do rather poorly, whilst the unrestricted Hartree–Fock approach does remarkably well in the large R regime. There have also been many theoretical studies of 2D quantum dots in a variety of confining potentials, which differ in the shape of the boundary (e.g. circular or polygonal), or the curvature of the potential (harmonic or hard walled)—for an interesting review see [16]. Mikhailov [17] has examined, using exact diagonalization, a three-electron parabolically confined 2D system (quantum-dot 'lithium'), and the crossover from Fermi liquid behaviour to a Wigner molecule. An alternative benchmark method is the diffusion quantum Monte Carlo method (as applied to quantum dots; see [18]). The emphasis on the 2D systems no doubt comes from the experiment, where the 2D confinement of a electron gas in a semiconductor heterostructure through electrostatic gating is feasible. On the other hand, such few-electron quantum systems serve as a 'playground' [16] in which to study interacting electron physics; we view our model in this vein. The three-dimensional nature of it could be relevant to real systems—for example, by providing insight into the crossover between Fermi liquid and Wigner molecule behaviour in 3D systems. However, we admit that the specific experimental realization of our model could be challenging.

In this paper we present a generalized configuration interaction algorithm for computing the ground and low lying states of N interacting electrons confined through an infinite spherical potential of radius R. It is organized in the following way. In section 2 we present the general

methodology employed. In section 3 we present results for the ground and low lying energetic states of the three-, four- and five-electron systems. In section 4 we give conclusions.

2. Method

The many-body Hamiltonian is given by (Hartree atomic units $\hbar = m_e = e^2 = 1$ are used throughout)

$$\hat{H} = \sum_{i=1}^{N} \left(-\frac{1}{2}\nabla_i^2 + \hat{v}_{\text{ext}}(\mathbf{r}_i) \right) + \sum_{i<j} \frac{1}{|\mathbf{r}_i - \mathbf{r}_j|}, \tag{1}$$

where the 3D external potential is defined through

$$\hat{v}_{\text{ext}}(\mathbf{r}) = \begin{cases} 0, & r < R, \\ \infty, & r \geqslant R. \end{cases} \tag{2}$$

To solve this problem we expand the many-body wavefunction as a linear combination of Slater determinants:

$$\begin{aligned} \Psi_i(\mathbf{x}_1, \mathbf{x}_2, \ldots, \mathbf{x}_N) &= \sum_j c_{ij} \Phi_j(\mathbf{x}_1, \mathbf{x}_2, \ldots, \mathbf{x}_N) \\ &= \sum_j c_{ij} |\eta_{n_1}(\mathbf{x}_1)\eta_{n_2}(\mathbf{x}_2)\cdots\eta_{n_K}(\mathbf{x}_N)\rangle, \end{aligned} \tag{3}$$

where the spin orbital $\eta_{\mathbf{n}}$ has the functional form

$$\eta_{nlms}(\mathbf{r}, \sigma) = N_{nl}\, j_l(\alpha_{nl} r) Y_{lm}(\theta, \phi)\delta_{\sigma,s} \tag{4}$$

and the j in equation (3) is shorthand for the particular determinant in question. We generate, given a user supplied list, any desired set of these functions. Selection of functions in this way allows us to restrict our attention to those that specifically contribute in the determinantal expansion. For clarity we shall take the total set of basis functions used, for example, 1f2d3p4s, to mean all functions 1s, 1p, 1d, 1f, 2s, 2p, 2d, 3s, 3p and 4s, inclusive.

Once we have specified a set of basis functions, we ladder them energetically. This laddering procedure is done with respect to the one-particle energies; these are found to order such that $1s < 1p < 1d < 2s < 1f < 2p < \cdots$ [19]. Having ordered the basis functions appropriately we construct a reference determinant out of the N lowest energy orbitals. We note that the reference state in the configuration interaction is usually the HF determinant; however, we find that a determinant constructed from the N lowest orbitals is a good choice for this system.

Given this reference determinant, we generate all possible excitations from it. The total number of such states is given by the binomial coefficient of N, the number of electrons and $2K$, the total number of spin orbitals; the size of the determinant space increases exponentially as a function of K. In order to reduce this space we apply some restrictions to the determinants included in the expansion. Recalling that the many-body wavefunction is an eigenfunction of both L_z and S_z, and that the total spin or angular momentum projection quantum number, for any given determinant, is given by

$$\begin{aligned} M_L &= \sum_i^N m_l(i), \\ M_S &= \sum_i^N m_s(i), \end{aligned} \tag{5}$$

we label the CI wavefunction (equation (3)) with the appropriate M_L and M_S quantum numbers.

Having generated the determinant space we construct the matrix representation of the Hamiltonian. In computing the matrix elements $\langle D|H|D'\rangle$ (where D and D' represent determinants in equation (3)), one takes advantage of the well-known Slater–Condon rules [20, 21] as applied to an orthogonal one-electron basis. This reduces the problem to terms involving only one- and two-electron integrals, the forms of which have been detailed in [11]. The Hamiltonian matrix is diagonalized using the Pollard–Friesner algorithm [22], which is an efficient iterative method based on Lanczos recursion, to obtain a user-specified number of the extremal eigenvectors of a Hermitian matrix. The diagonalization of the Hamiltonian, in all but the largest of calculations, did not present a significant computational bottleneck.

2.1. Calculation of the N-electron density, second-order density matrix and physical exchange–correlation hole

Given the CI wavefunction as defined through equation (3), we seek to calculate properties which will help us understand the physics of these many-electron systems. We shall consider the electron density and many-body properties such as the second-order density matrix and the physical exchange–correlation hole.

2.1.1. Electron density. The electron density of the system is given by

$$n(\mathbf{r}) = \langle \Psi | \hat{n}(\mathbf{r}) | \Psi \rangle, \tag{6}$$

with the one-body number density operator, $\hat{n}(\mathbf{r})$, being defined through

$$\hat{n}(\mathbf{r}) = \sum_i \delta(\mathbf{r} - \mathbf{r}_i). \tag{7}$$

Contributions arising from determinants that differ by two or more spin orbitals is zero. For those determinants that differ by one spin orbital the subsequent contribution is given by the product of the orbitals that they differ by $(\eta_n^{*\prime}(\mathbf{r})\eta_n(\mathbf{r}))$. When considering determinants that differ by no spin orbital (i.e. they are the same determinant), the resulting contribution to the electronic density is $\sum_i^N \eta_i^*(\mathbf{r})\eta_i(\mathbf{r})$.

2.1.2. The second-order density matrix and exchange–correlation hole. We know that for the two-electron problem the physical exchange–correlation hole can be written solely in terms of the two-electron wavefunction [23]. In the case of an N-electron system there is no such simple relationship with the many-body wavefunction. We can relate the physical exchange–correlation hole to the second-order density matrix such that

$$n_{\mathrm{xc}}(\mathbf{r}, \mathbf{r}') = \frac{2n_2(\mathbf{r}, \mathbf{r}')}{n(\mathbf{r})} - n(\mathbf{r}') \tag{8}$$

where the spinless second-order density matrix is defined through

$$n_2(\mathbf{r}, \mathbf{r}') = \frac{N(N-1)}{2} \int \cdots \int |\Psi|^2 \, \mathrm{d}s_1 \, \mathrm{d}s_2 \, \mathrm{d}\mathbf{x}_3 \cdots \mathbf{x}_N. \tag{9}$$

Thus, this many-body density matrix, together with the electron density, yields the physical exchange–correlation hole. Although this is formally a six-dimensional object, we specify as input the position of $\mathbf{r}$ and calculate a three-dimensional n_2 as a function of $\mathbf{r}'$. After computing n_2 and n_{xc} we ensure that the latter object satisfies a sum rule, i.e. integrates to -1, and that the integral of the second-order density matrix yields the value of the density at the reference point:

$$n(\mathbf{r}) = \frac{2}{N-1} \int n_2(\mathbf{r}, \mathbf{r}') \, \mathrm{d}\mathbf{r}'. \tag{10}$$

This quantity allows us to probe the spatial correlation between the electrons as a function of the reference particle position $\mathbf{r}$ and sphere radius R for not only the ground state, but low lying excited states as well. This information will be interesting to researchers in the field of functional development, as the shape of the exchange–correlation hole is often a key tool in novel functional design [24].

2.1.3. Natural orbitals. The natural orbitals are eigenfunctions of the one-body density matrix, and their associated eigenvalues are occupation numbers which range from 0 to 1. The natural orbitals provide extremely interesting insight into the structure of the many-body wavefunction $\Psi_{M_S M_L}(\mathbf{x}_1, \ldots, \mathbf{x}_N)$, and are a natural, correlated, single-particle basis.

We compute the one-body reduced density matrix $\gamma_1(\mathbf{x}, \mathbf{x}')$ [23] and perform the resulting integration over determinants using the Slater–Condon rules. We then form a matrix representation of γ_1 in terms of the original one-particle basis functions (equation (4)). The resulting equation is viewed as a sum of diagonal and off-diagonal terms, where, in the latter case, j' can *only* be a single excitation from j:

$$\langle \eta_{\mathbf{n}} | \gamma_1 | \eta_{\mathbf{n}'} \rangle = N \left[\sum_{j \in \mathbf{n}} c_j^2 \delta_{\mathbf{n}\mathbf{n}'} + \sum_j c_j c_{j'(j)} \right]. \tag{11}$$

The eigenvalues and eigenvectors of this matrix are the occupation numbers and the natural orbitals of the system respectively. It is then straightforward, using the natural orbitals, to perform a total angular momentum decomposition of the many-body wavefunction.

3. Results

3.1. Three-electron system

As the many-body wavefunction is an eigenfunction of both $\hat{L}^2$ and $\hat{S}^2$, we can assign term symbols to it. For a three-electron system we find that the two lowest competitive states are the ^{2}P and ^{4}P.

The first question to be addressed is which of the two is the ground state as a function of R. Based on a simple kinetic energy versus potential energy consideration, one might guess that the ^{2}P (being derived from s^2p) would be the ground state at small R, and the ^{4}P (derived from sp^2) to be the ground state at large R, the rationale for this being that such hybrid orbitals form an equilateral triangle, precisely the shape required to minimize the Coulomb repulsion between the three electrons. In table 1 below we present the energies of these two states for a range of sets of spin orbitals, here $R = 5$. The maximum sized set consisted of 182 orbitals and both the ^{2}P and ^{4}P energies are well converged with respect to the basis up to 1 part in 10^5. Note also that the states are well resolved.

In table 2 we present the four largest basis set energies for the $R = 20$ system; the ^{2}P and ^{4}P energies remain well separated with $E(^4\mathrm{P}) > E(^2\mathrm{P})$. For large R the convergence of these states is seen to depend sensitively upon the basis. For a minimal basis (1p) at $R = 20$ we find $E(^2\mathrm{P}) = 0.266$, while $E(^4\mathrm{P}) = 0.260$. In other words, for a minimal basis, the ^{4}P does indeed have a lower energy than the ^{2}P. An increase in the basis size to the 1d2p level reverses this order; subsequent increases lower the energy variationally without altering the ordering. Therefore, we arrive at an important result which contradicts our simple expectation that, in the large R limit, the ^{4}P state should be the ground state. In other words, the configuration interaction more effectively lowers the energy of the ^{2}P state compared to the ^{4}P state. By performing a natural orbital analysis [13], one can show that the ^{2}P state evolves from s^2p to a more complex configuration with depleted s content, and increased p and d content.

Table 1. Showing the energy, in atomic units, of the ^{2}P and ^{4}P states in the three-electron problem. We present results for $R = 5$. We indicate the basis set by giving l_{max} for each n; e.g. 1d2p implies a basis set with 1s, 1p, 1d, 2s and 2p functions, inclusive.

Basis set	No of spin orbitals	No of determinants	^{2}P	^{4}P
1g	50	19 600	1.675 4436	1.762 4862
1g2g	100	161 700	1.629 8614	1.735 5872
1g2g3g	150	551 300	1.629 2023	1.735 4495
1g2g3g4s	152	573 800	1.629 1866	1.735 4472
1g2g3g4p	158	644 956	1.629 1716	1.735 4412
1g2g3g4d	168	776 216	1.629 1613	1.735 4400
1g2g3g4f	182	988 260	1.629 1534	1.735 4392

Table 2. Showing the energy, in atomic units, of the ^{2}P and ^{4}P states in the three-electron problem. Here $R = 20$.

Basis set	^{2}P	^{4}P
1g2g3g4s	0.225 090 04	0.227 488 24
1g2g3g4p	0.225 084 07	0.227 478 83
1g2g3g4d	0.225 083 82	0.227 478 66
1g2g3g4f	0.225 083 78	0.227 478 65

The p content does not reach 2. The higher angular momentum orbitals (d in particular) play a crucial role in stabilizing the ^{2}P state.

In figure 1 we consider the ground state electron density. The most important point to notice is that the densities are *not* spherically symmetric, and, being P states and degenerate, they are labelled according to their M_L values. We present the ^{2}P $M_L = \pm 1$ (left) and ^{2}P $M_L = 0$ (right) densities for $R = 1, 5$ and 20. The $M_L = \pm 1$ densities are oriented such that the xy plane is shown, whilst in the $M_L = 0$ instance we show the yz plane. In the former case the maximal contour is highlighted. This has a well-developed ring structure to it and the radii of this shape are seen to increase with increasing R. For $M_L = 0$ the maximal density is located in two regions, equidistant from the origin, at opposite points along the z-axis. Figure 2 shows, for $R = 1$ and 20, the ^{4}P $M_L = \pm 1$ (left) and ^{4}P $M_L = 0$ (right) excited state densities for this three-electron system. The structures of the densities shown in figures 1 and 2 are easily understood in terms of the M_L quantum number and the principal character of the CI wavefunction as revealed through the natural orbital analysis.

In figure 3 we compute the function E_c/E for a number of values of $r_s = R/N^{1/3}$, where the correlation energy, E_c, is defined in terms of the UHF ground state energy:

$$E_c = E - E_{UHF}. \tag{12}$$

The rationale for this is that $|E_c/E|$ measures the *relative* error in the UHF energies. This is important since both E and $-E_c$ are positive, and decreasing, functions of r_s, and we need a measure of the magnitude of E_c compared to the exact total energy E. We note that for small r_s the $M_s = \frac{1}{2}$ UHF state is a reasonable approximation to the exact one. We observe a transition in the UHF ground state to the $M_s = 3/2$ state at $r_s = 7.12$. For small r_s, E_c/E is a linear increasing function of r_s. $|E_c/E|$ achieves a maximum value of $\sim$0.048 at $r_s \sim 6.9$, and thereafter decreases, reaching an asymptotic value of $\sim$0.04 for large r_s. This indicates that the UHF description of the deep Wigner molecule regime is better than the crossover regime. The high spin UHF state helps to keep the electrons apart through their Fermi holes.

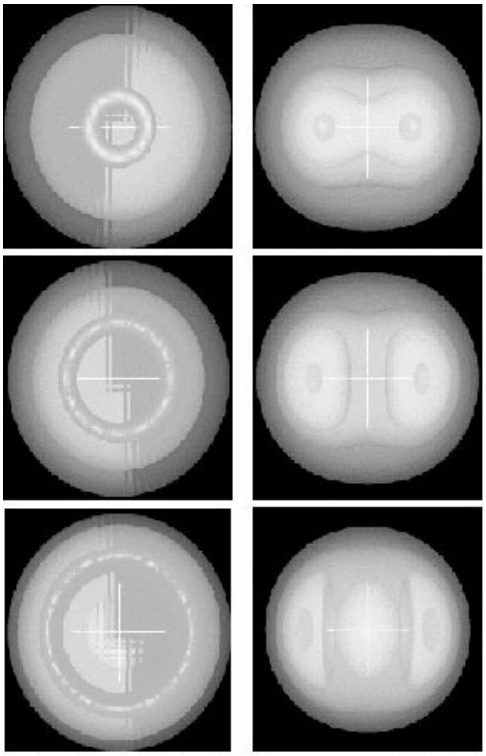

Figure 1. Left: the ^{2}P $M_L = \pm 1$ three-electron density as a function of R; the xy plane is shown. From top to bottom we consider $R = 1, 5$ and 20. Right: the ^{2}P $M_L = 0$ three-electron density for the same range of sphere sizes; here, the yz plane is shown. The ^{2}P FCI wavefunction has predominantly s^2p character.

To illustrate the change in the pair correlation of the system as a function of r_s we have computed the two-body density matrix. We consider the ^{2}P $M_L = \pm 1$ state (having a ring-like density as seen in figure 2). A reference particle is placed within the region of high density, halfway along the x-axis at $(0.5R, \pi/2, 0)$. We consider $R = 1$ (weakly correlated) and $R = 20$ (Wigner molecule regime) and include these as insets to figures 3(a)–(c) respectively. The figures are oriented such that the reader is looking down the x-axis. The $R = 1$ state exhibits a single peak (maximal contour shown, highlighted in white) diametrically opposite the reference particle (highlighted with a dot, in the centre of the image), implying that the most likely location of a particle is roughly opposite the reference particle. This is the situation that one would expect in a liquid-like system. As R increases this peak splits into two broad peaks; indeed the deepening of the value of $|E_c/E|$ correlates with the splitting of the single peak into two well-resolved peaks. Inset (b) shows the density matrix for the 'most correlated' value of $r_s \sim 6.9$.

Changes in the shape of the second-order density matrix as a function of reference particle position are investigated in figure 4; we show $n_2(\mathbf{r}, \mathbf{r}')$ for a quarter of the way along the z-axis i.e. $\mathbf{r} = (0.25R, 0, 0)$. We see that the maximal contour, in all cases, is azimuthally symmetric, entirely consistent with the densities observed for these systems. Also, there appears to be, for increasing R, an enhancement of probability around the reference particle, most clearly seen in the ^{4}P case.

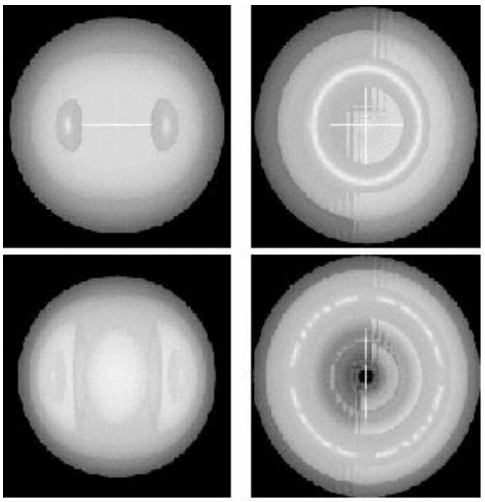

Figure 2. Left: the ^{4}P $M_L = \pm 1$ three-electron density as a function of R; the yz plane is shown. Right: the ^{4}P $M_L = 0$ three-electron density for the same range of sphere sizes with the xy plane shown. We consider $R = 1$ (top) and 20 (bottom).

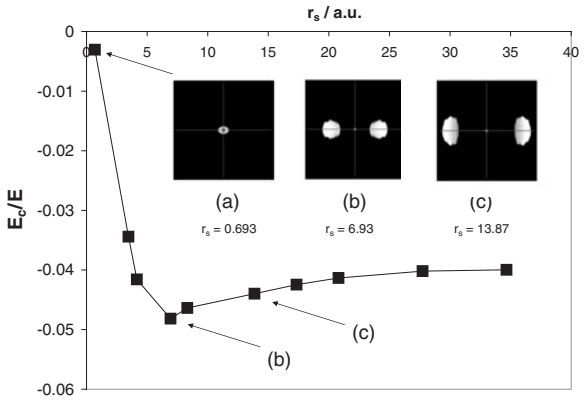

Figure 3. The ratio E_c/E is computed using the UHF ground state energy. We observe a maximally correlated region ($r_s = 5$–10) which corresponds to the formation of a Wigner-like state. The insets (a)–(c) show two-body density matrices, $n_2(\mathbf{r}, \mathbf{r}')$, for $R = 1$, 10 and 20 respectively. The reference particle, highlighted at the centre of the image, is placed at $(0.5R, \pi/2, 0)$, halfway along the x-axis. In all cases, near maximal contours are shown. The contours used for insets (a)–(c) are 1.85 (1.875), 1.2×10^{-3} (1.17×10^{-3}) and 1.29×10^{-4} (1.22×10^{-4}). The numbers in parentheses correspond to the maximal contours calculated.

For $R = 20$ a breakdown of the total energy into its kinetic and Coulombic contributions is shown below in table 3. For this large value of R the ^{4}P (high spin) state has a lower Coulomb energy than the corresponding ^{2}P state. However, the kinetic energy is sufficiently higher to offset this gain. This table indicates the delicate balance between $\langle \Delta T \rangle$ and $\langle \Delta U \rangle$ for the two states in this system.

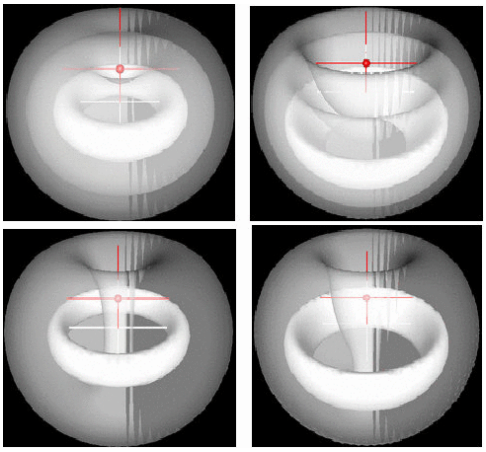

Figure 4. The second-order density matrix for $R = 1$ and 20 for the ^{2}P $M_L = \pm 1$ state (left) and the ^{4}P $M_L = 0$ state (right). The reference particle is shown with a small, solid dot and is placed along the z-axis at $(0.25R, 0, 0)$. The figures are oriented such that the xz plane is shown.

Table 3. Breakdown of the kinetic and potential energies of the CI wavefunctions for the three-electron system in the large sphere limit ($R = 20$), calculations have been performed using the 1g2g3g4f basis set.

$N = 3$	$\langle T \rangle$	$\langle U \rangle$	$\langle E \rangle$
(^{2}P)	0.0751	0.1500	0.2251
(^{4}P)	0.0794	0.1481	0.2275

3.2. Four-electron system

In the high density regime the four-electron system is well described by the electronic configuration s^2p^2. The term symbols arising from such a configuration are ^{3}P, ^{1}D and ^{1}S. Ordering these states energetically using Hund's rules we find $^3\mathrm{P} < {}^1\mathrm{D} < {}^1\mathrm{S}$. We find all of these states in their correct ratios (9:5:1), ordered in the correct way for small R. Increasing the size of the sphere leads to an excited state becoming competitive with the ^{3}P ground state. This excited state is found to be fivefold degenerate with $L = 0$; we identify it as a ^{5}S state and its principal determinantal configuration is sp^3. The energy convergence as a function of basis set, for $R = 5$, is detailed in table 4. The largest system of study—the 1g2g3p basis—although giving the lowest energy for $R = 5$, actually does not perform as well as the 1g2f3d4s basis at $R = 20$; for consistency, at all R, we use this more 'flexible' basis. This illustrates important changes in the system. At $R = 20$ the ^{5}S state is now the ground state; *we observe a transition to a fully spin-polarized ferromagnetic ground state as a function of increasing* R. Indeed the ^{5}S state cascades down from being a low lying excited state to being competitive with the s^2p^2 manifold, with the final $^3\mathrm{P} \rightarrow {}^5\mathrm{S}$ crossover occurring at $R = 13.79$ ($r_s = 8.69$). This transition is seen most clearly in figure 5 where we plot $(E_X(R) - E_{^5S}(R)) \cdot r_s^2$ for $X = {}^3$P (configuration interaction), and the UHF states $M_s = 0$, 1 and 2. The energy difference between the ^{3}P and ^{5}S states decreases rapidly, changing sign at $r_s \approx 8.69$, and then increasing, albeit slowly, as a function of R. The UHF solutions undergo an $M_s = 0 \rightarrow 2$ transition at $r_s = 3.81$, foreshadowing the transition in the exact ground state at a somewhat higher density.

As distinct from the $N = 3$ system, therefore, the $N = 4$ system shows a spin transition to a high spin state, both at the UHF level and in the FCI, albeit at different radii. The function

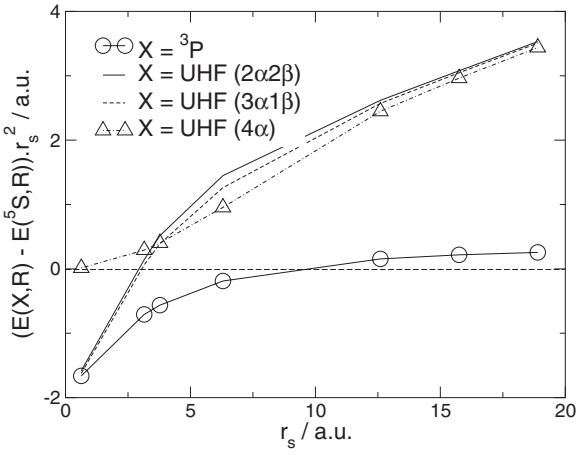

Figure 5. The energy difference between ^{5}S and the ^{3}P configuration interaction energies. At $r_s \approx 8.7$, ^{5}S becomes the ground state. We also show the differences between the unrestricted Hartree–Fock energies for $M_s = 0$, 1 and 2. The UHF high spin state is stabilized at a much higher density, $r_s = 3.81$.

Table 4. Showing the energy, in atomic units, of the ^{3}P and ^{5}S states in the four-electron problem. Here $R = 5$.

Basis set	No of spin orbitals	No of determinants	^{3}P	^{5}S
1p	8	70	2.966 240 55	2.970 947 87
1d	18	3 060	2.908 671 59	2.948 259 97
1f	32	35 960	2.901 870 32	2.943 739 73
1g	50	230 300	2.901 271 32	2.943 361 76
1g2f	82	1749 060	2.805 822 82	2.875 801 54
1g2f3s	84	1929 501	2.804 465 52	2.875 607 41
1g2f3p	90	2555 190	2.803 949 06	2.875 170 81
1g2f3d	100	3921 225	2.803 870 82	2.875 156 41
1g2f3d4s	102	4249 575	2.803 829 61	2.875 151 80
1g2g3s	102	4249 575	2.804 269 61	2.875 537 89
1g2g3p	108	5359 095	2.803 760 60	2.875 104 43

E_c/E, where $E_c = E(\mathrm{FCI}) - E(\mathrm{UHF})$, is therefore expected to have discontinuous behaviour as both the FCI ground state and the UHF solutions undergo spin transitions. This is shown in figure 6 (bold curve). The FCI and UHF (RHF) calculations were performed using the 1g2f3d4s and 1f2f3f basis sets respectively. The kink at $r_s = 3.81$, giving rise to a marked local maximum in $|E_c/E|$, is due to the UHF spin transition, which also signals the onset of Wigner molecule formation. One can also compute $|E_c/E|$ defined with respect to the low spin and high spin UHF and FCI states separately, for which one expects smooth behaviour. In the case of the $M_s = 1$ state, one finds that for small r_s, $|E_c/E|$ is larger than the corresponding high spin state, indicating that the correlation energies in the low spin states are larger than the corresponding high spin state. This is another indication that the configuration interaction more effectively lowers the energy of the low spin configurations than the high spin ones. Nevertheless, the maximum UHF relative error is less than 5%, by contrast to the RHF relative error (shown in the inset) which grows with increasing r_s, exceeding 20% at large r_s. The attenuating UHF

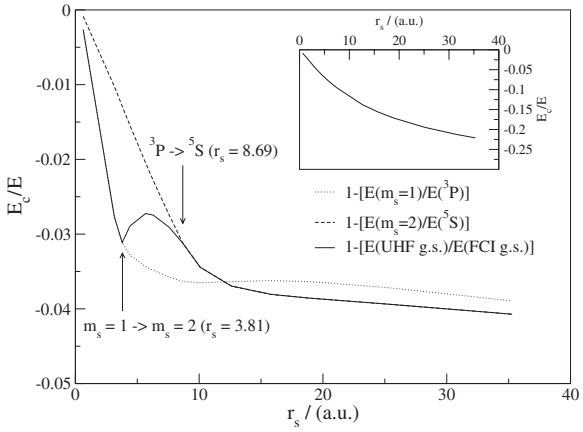

Figure 6. E_c/E against r_s for the four-electron system. We compute this quantity for both UHF states and for the overall UHF ground state. The inset shows the E_c/E function corresponding to the RHF eigenvalues.

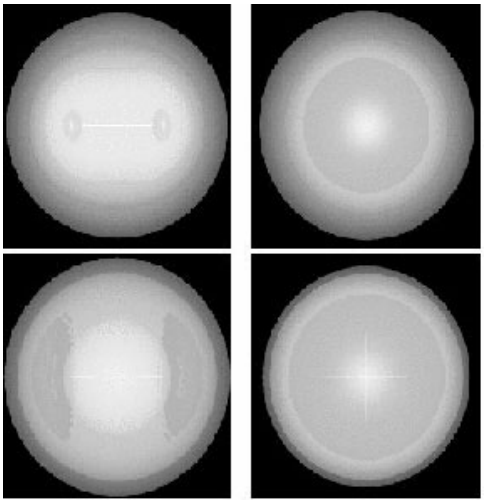

Figure 7. Three-dimensional plots of the electronic density for the ^{3}P $M_L = \pm 1$ (left) and ^{5}S (right) four-electron states. In the former instance the yz plane is shown. We consider $R = 1$ (top) and 20 (bottom).

error is an indication that the Wigner molecule limit is reasonably well captured by the UHF approximation.

The densities of the competitive states are shown in figure 7—the ^{3}P $M_L = \pm 1$ (left) and ^{5}S (right) for the $R = 1$ and 20 sized spheres; in the ^{3}P case the yz plane is shown. The spherical symmetry of the ^{5}S state is seen most clearly with the maximal contour (highlighted) precessing towards the edge of the sphere with increasing R. The ^{3}P $M_L = 0$ state has a ring-like structure about the z-axis. As in the three-electron case, the radii of the rings are seen to increase with increasing sphere size.

An investigation of the second-order density matrix for this system (figure 8) indicates that at high density ($R = 1$) the ^{3}P $M_L = \pm 1$ state (left) is weakly correlated with the likeliest place to find the particles being opposite the reference position. In this figure the reference particle

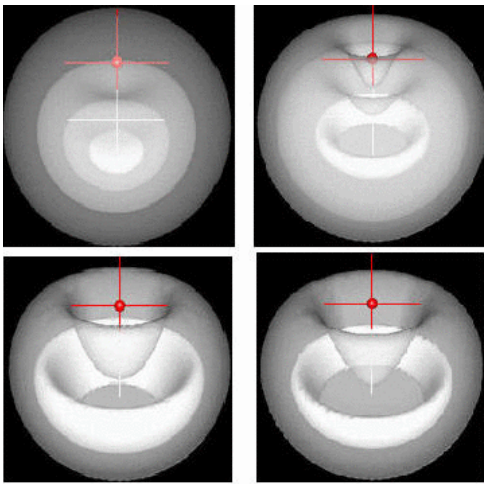

Figure 8. The second-order density matrix for $R = 1$ and 20 for the ^{3}P $M_L = \pm 1$ state (left) and the ^{5}S $M_L = 0$ state (right). The reference particle is highlighted and is placed at $(0.5R, 0, 0)$. The figures are oriented such that the xz plane is shown. For completeness we note that both $R = 1$ figures show maximal contours with values of $\sim$2 and enclosing, minimal, contours of $\sim$0.1. For the larger, $R = 20$, systems the density matrices have maximal contours $\sim \times 10^{-4}$ with minimal enclosing contours of $\sim \times 10^{-5}$. These values are characteristic of all systems examined.

is placed halfway along the z-axis at $\mathbf{r} = (0.5R, 0, 0)$ and is highlighted. Upon increasing R, the system develops a ring structure opposite the reference particle. This is also seen in the ^{5}S state (right), where this structure exists even at $R = 1$.

To probe the correlated motion of the system we calculate the physical exchange–correlation hole and the second-order density matrix for the ^{3}P $M_L = 0$, $R = 20$ system. This is shown in figure 9. In the topmost panel these objects are shown for $\mathbf{r}$ being halfway along the x-axis; this corresponds to placement of the reference particle in a region of high electron density (due to its ring-like structure). The spatially anisotropic shape of the second-order density matrix, which exhibits broader peaks in the xy plane, reflects the strongly correlated motion of the particles. Fixing $\mathbf{r} = (0.5R, \pi/2, 0)$, two electrons are found equidistant from it (inside the ring of high electron density) with the remaining particle, instead of being frustrated in this arrangement (due to enhanced Coulomb repulsion), choosing to move in the xz plane. This is mirrored in n_{xc} where the xy anisotropy is clear in the maximal positive region. Conversely, with $\mathbf{r}$ halfway along the z-axis, $(0.5R, 0, 0)$, there is no spatial preference and the remaining electrons are found in a ring diametrically opposite the reference particle.

From the three- and four-electron systems studied thus far, it is clear that an analysis of the many-body properties yields useful insight into the structure of the strongly correlated regimes found at large R. To summarize: for $\mathbf{r}$ along the z-axis the second-order density matrix preserves the ring-like structure diametrically opposite the reference particle in both systems. However, for $\mathbf{r}$ along the x-axis the collective interactions reveal something about the correlation between the particles. In the case of three electrons the two remaining particles are found in the xz plane in a triangular arrangement as would be expected from a classical Coulombic analysis. In the four-electron case this is not possible and the frustrated motion of the system is clearly evinced. This has also been noted from a detailed population analysis of the angular momentum of the three- and four-electron systems, where an interesting link is posited between hybrid orbital formation and Wigner crystallization [13].

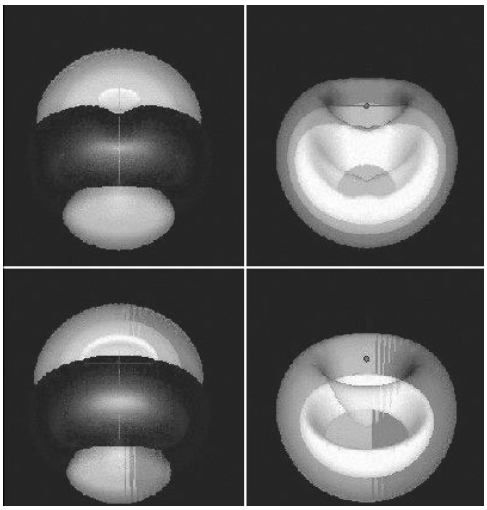

Figure 9. Here we plot both the physical exchange–correlation hole (left) and the second-order density matrix (right) for the four-electron ^{3}P $M_L = 0$ $R = 20$ system for the reference particle placed at $(0.5R, \pi/2, 0)$ (top, xy plane shown) and $(0.5R, 0, 0)$ (bottom, xz plane shown). The exchange–correlation holes have been rotated to highlight the anisotropic structure in the positive region.

Table 5. Breakdown of the kinetic and potential energies of the CI wavefunctions for the four-electron system in the large sphere limit ($R = 20$); calculations have been performed using the 1g2f3d4s basis set.

$N = 4$	$\langle T \rangle$	$\langle U \rangle$	$\langle E \rangle$
(^{3}P)	0.1199	0.2986	0.4184
(^{5}S)	0.1210	0.2965	0.4175

A breakdown of the total four-electron energy is shown, in table 5. We find a Coulomb dominance over the kinetic energy, as for $N = 3$, and a lower ^{5}S $\langle U \rangle$ as compared to that for ^{3}P. It is this difference, despite the increased kinetic energy for this state, that leads to a decreased ^{5}S total energy.

3.3. Five-electron system

Finally, we turn our attention to the five-electron problem. In figure 10 we examine the energy convergence as a function of basis set size for the $R = 20$ five-electron, ^{4}S and ^{6}D states where the ^{4}S term symbol arises from an s^2p^3 electronic configuration. The energetically competitive ^{6}D state is of interest, as it corresponds to the lowest of the sp^3d manifold associated with a trigonal bi-pyramid structure—the classically predicted arrangement which would minimize the localized electron–electron repulsion for large R.

We observe that the two states are well resolved with $^4\mathrm{S} < {}^6\mathrm{D}$, even for large R. Indeed this is clearly shown in figure 11 where the difference between the states is seen to increase smoothly (after having first decreased). We note that the five-electron UHF state is ferromagnetic for sufficiently large R.

Given that the ground state is spherically symmetric, radial plots suffice for describing the density, and also allow comparison with other similar ground state densities. For example, one

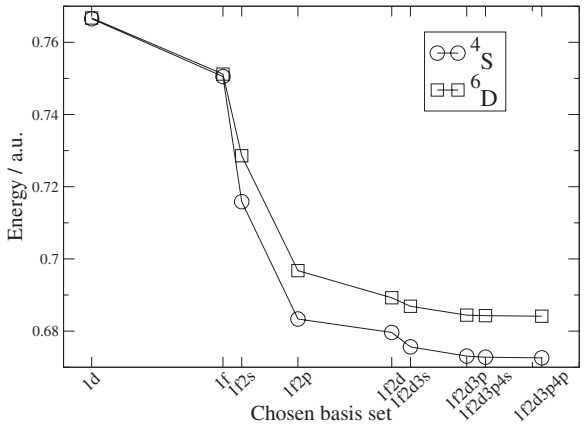

Figure 10. The convergence of the ^{4}S and ^{6}D five-electron states as a function of basis set. The largest calculation with 66 spin orbitals contained 8936 928 determinants in the full space. We note that, interestingly, for very small basis sets the resolution between states is poor.

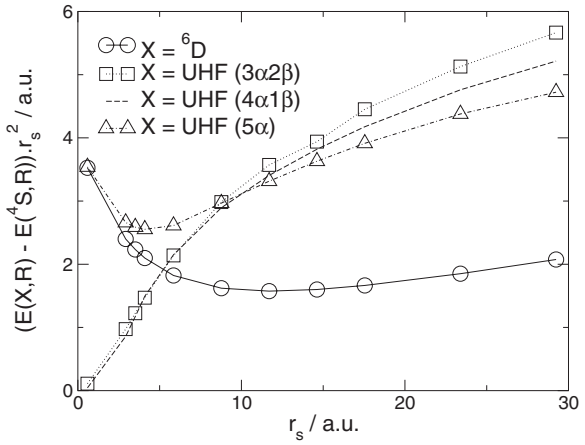

Figure 11. The energy difference, in atomic units, between the ^{4}S (five-electron ground state) and configuration interaction ^{6}D and the $M_s = 1/2$, $3/2$ and $5/2$ unrestricted Hartree–Fock energies calculated at the 1f2f3f basis set level.

can ask the question: suppose we add an electron to a four-electron system at fixed R, how will the electron density rearrange? We plot the spherically averaged density as a function of distance from the origin for the ^{5}S ($N = 4$), ^{4}S ($N = 5$) and ^{1}S ($N = 2$) states in figure 12. We see that for large R the four- and five-electron densities are very similar, with almost identically positioned maxima. The ^{1}S ($N = 2$) state for $R = 50$ illustrates that the effect of increasing the number of electrons is to narrow the width of the density distribution and shift the maxima towards the edge of the sphere (as a result of enhanced Coulomb repulsion).

4. Conclusions

In this paper we have presented a FCI and UHF study of confined interacting electrons, where the confining potential is an infinite spherical box, of radius R. We discuss the ground and

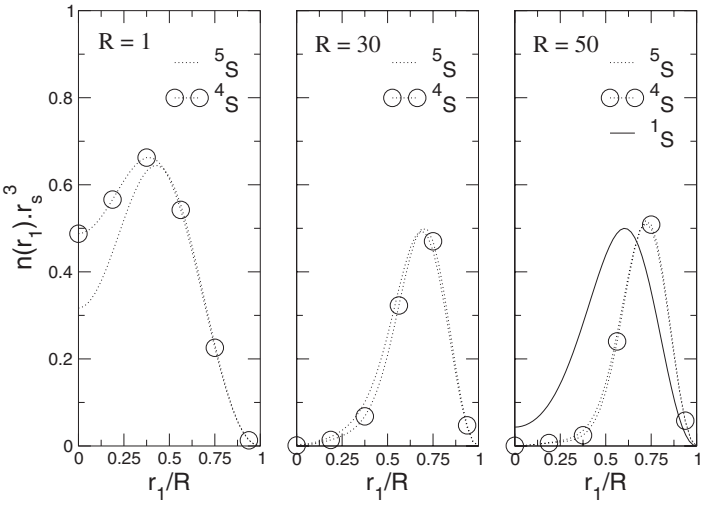

Figure 12. The four- and five-electron *singlet* densities as a function of R. We see that for large R the densities are essentially the same. For comparison we also include the ^{1}S two-electron $R = 50$ density.

low lying excited state solutions for the three-, four- and five-electron systems as a function of the confining sphere radius. Given the properties of the many-body wavefunction we assign electronic term symbols to the solutions and find that for small R the ^{2}P, ^{3}P and ^{4}S symbols label the respective $N = 3, 4$ and 5 electron ground states. In the four-electron problem a mobile ^{5}S state is seen to become the ground state at $R \sim 14$. It remains the lowest energy state for all subsequent R considered. This transition to a fully spin-polarized state, as a function of increasing R, is not observed for the $N = 3$ and 5 systems.

Comparison of the UHF energies with respect to the FCI solutions leads to the conclusion that the relative error caused by the independent-electron approximation is most severe in the crossover regime where the electron system is changing from a liquid droplet to a Wigner molecule. The pair-correlation functions and exchange–correlation holes exhibit marked yet characteristic changes in this difficult regime. The subtle balance between kinetic and Coulomb energy exhibited by these systems, together with the flexibility to tune the electron correlation present, suggests that they could provide challenging and useful benchmarks for post-Hartree–Fock and DFT methods.

References

[1] Trail J R, Towler M D and Needs R J 2003 *Phys. Rev.* B **68** 045107
[2] Yannouleas C and Landman U 1999 *Phys. Rev. Lett.* **82** 5325
[3] Räsänen E *et al* 2003 *Phys. Rev.* B **67** 035326
[4] Akbar S and Lee I-H 2001 *Phys. Rev.* B **63** 165301
[5] Kais S *et al* 1993 *J. Chem. Phys.* **99** 417
[6] Taut M 1993 *Phys. Rev.* A **48** 3561
[7] Filippi C, Umrigar C J and Taut M 1993 *J. Chem. Phys.* **100** 1290
[8] Laufer P M and Krieger J B 1986 *Phys. Rev.* A **33** 1480
[9] Taut M *et al* 2003 *J. Chem. Phys.* **118** 4861
[10] Alavi A 2000 *J. Chem. Phys.* **113** 7735
[11] Thompson D C and Alavi A 2002 *Phys. Rev.* B **66** 235118
[12] Jung J and Alvarellos J E 2003 *J. Chem. Phys.* **118** 10825

[13] Thompson D C and Alavi A 2004 *Phys. Rev.* B **69** 201302
[14] Thompson D C and Alavi A 2004 at press
[15] Jung J, García-González P, Alvarellos J E and Godby R W 2004 *Phys. Rev.* A **69** 052501
[16] Riemann S M and Manninen M 2002 *Rev. Mod. Phys.* **74** 1283
[17] Mikhailov S A 2002 *Phys. Rev.* B **65** 115312
[18] Pederiva F, Umrigar C J and Lipparini E 2000 *Phys. Rev.* B **62** 8120
[19] Landau L D and Lifshitz E M 1958 *Quantum Mechanics: Nonrelativistic Theory* (Reading, MA: Addison-Wesley)
[20] Slater J C 1929 *Phys. Rev.* **34** 1293
[21] Condon E U 1930 *Phys. Rev.* **36** 1121
[22] Pollard W T and Friesner R A 1993 *J. Chem. Phys.* **99** 6742
[23] Parr R G and Yang W 1989 *Density-Functional Theory of Atoms and Molecules* (Oxford: Oxford University Press)
[24] Perdew J P, Burke K and Yang Y 1998 *Phys. Rev.* B **57** 14999